Title

Characterization of growth and development of sorghum genotypes with differential susceptibility to Striga hermonthica

Journal

Journal of Experimental Botany, 72(22)

ISSN

0022-0957

Authors

Kawa, Dorota

Taylor, Tamera

Thiombiano, Benjamin

et al.

Publication Date

2021-12-04

DOI

10.1093/jxb/erab380

Journal of Experimental Botany, Vol. 72, No. 22 pp. 7970–7983, 2021
https://doi.org/10.1093/jxb/erab380 Advance Access Publication 19 August 2021
This paper is available online free of all access charges (see https://academic.oup.com/jxb/pages/openaccess for further details)

RESEARCH PAPER

Characterization of growth and development of sorghum genotypes with differential susceptibility to *Striga hermonthica*

Dorota Kawa[1], Tamera Taylor[1,2], Benjamin Thiombiano[3], Zayan Musa[1], Hannah E. Vahldick[1], Aimee Walmsley[3], Alexander Bucksch[4,5,6], Harro Bouwmeester[3] and Siobhan M. Brady[1,*]

[1] Department of Plant Biology and Genome Center, University of California, Davis, Davis, CA 95616, USA
[2] Plant Biology Graduate Group, University of California, Davis, Davis, CA 95616, USA
[3] Plant Hormone Biology Group, Green Life Sciences Cluster, Swammerdam Institute for Life Science, University of Amsterdam, 1098 XH Amsterdam, the Netherlands
[4] Department of Plant Biology, University of Georgia, Athens, GA 30602, USA
[5] Institute of Bioinformatics, University of Georgia, Athens, GA 30602, USA
[6] Warnell School of Forestry and Natural Resources, University of Georgia, GA 30602, USA

* Correspondence: sbrady@ucdavis.edu

Received 24 February 2021; Editorial decision 13 August 2021; Accepted 17 August 2021

Editor: Ros Gleadow, Monash University, Australia

Abstract

Two sorghum varieties, Shanqui Red (SQR) and SRN39, have distinct levels of susceptibility to the parasitic weed *Striga hermonthica*, which have been attributed to different strigolactone composition within their root exudates. Root exudates of the Striga-susceptible variety Shanqui Red (SQR) contain primarily 5-deoxystrigol, which has a high efficiency for inducing Striga germination. SRN39 roots primarily exude orobanchol, leading to reduced Striga germination and making this variety resistant to Striga. The structural diversity in exuded strigolactones is determined by a polymorphism in the *LOW GERMINATION STIMULANT 1* (*LGS1*) locus. Yet, the genetic diversity between SQR and SRN39 is broad and has not been addressed in terms of growth and development. Here, we demonstrate additional differences between SQR and SRN39 by phenotypic and molecular characterization. A suite of genes related to metabolism was differentially expressed between SQR and SRN39. Increased levels of gibberellin precursors in SRN39 were accompanied by slower growth rate and developmental delay and we observed an overall increased SRN39 biomass. The slow-down in growth and differences in transcriptome profiles of SRN39 were strongly associated with plant age. Additionally, enhanced lateral root growth was observed in SRN39 and three additional genotypes exuding primarily orobanchol. In summary, we demonstrate that the differences between SQR and SRN39 reach further than the changes in strigolactone profile in the root exudate and translate into alterations in growth and development.

Keywords: Developmental delay, gibberellins, lateral root, metabolism, root system architecture, sorghum, *Striga hermonthica*, strigolactone.

Abbreviations: ABA, abscisic acid; AM, arbuscular mycorrhiza; LGS1, Low Germination Stimulant 1; SQR, Shanqui Red.

Introduction

Sorghum bicolor is one of the five most important cereal crops globally (Paterson *et al.*, 2009). Its adaptations to drought, heat, and low nutrient availability make sorghum especially important for agriculture in sub-Saharan Africa, where it is a staple food, feed, and forage (Mace *et al.*, 2013). Among sorghum strategies to withstand abiotic stresses, establishing interactions with arbuscular mycorrhiza (AM) fungi improves phosphate acquisition (Neumann and George, 2004). To recruit AM fungi, plants secrete strigolactones into the soil, carotenoid-derived compounds that induce AM hyphal branching (Akiyama *et al.*, 2005). Low nutrient concentration, primarily phosphate and nitrogen, induces strigolactone exudation (Jamil *et al.*, 2013), which ensures AM fungal recruitment (Bouwmeester *et al.*, 2007; Yoneyama *et al.*, 2007). While this plant–fungus communication system is beneficial for sorghum's performance in nutrient-depleted soils, the strigolactone signal can be hijacked by seeds of the parasitic 'witchweed', *Striga hermonthica* (Bouwmeester *et al.*, 2007). Striga is an obligate parasite and strigolactones are essential for its seed germination (Spallek *et al.*, 2013; Bouwmeester *et al.*, 2020). Co-option of strigolactone signaling by Striga ensures it germinates only in the presence of a host plant. The ability to sense the presence of strigolactones allows Striga seeds to stay dormant for years and makes Striga an extraordinarily successful parasite. After strigolactone perception, germinated Striga forms a haustorium that penetrates the roots of a host plant and establishes a connection between its own xylem and the xylem of the host plant, to deprive the host of water and nutrients (Spallek *et al.*, 2013). Striga infestation has a detrimental effect on a host plant and around 20% of sorghum yield is lost annually (Ejeta and Gressel, 2007).

Since strigolactones are essential for Striga parasitism, understanding their biosynthesis and functions is essential to combat Striga parasitism. More than 35 different strigolactones have been discovered across plant species, yet not all have the potential to induce Striga germination to the same extent (Wang and Bouwmeester, 2018). Among the five main strigolactones produced by sorghum, 5-deoxystrigol, sorgomol, sorgolactone, and strigol have high Striga germination stimulant activity, while orobanchol is a low germination stimulant (Awad *et al.*, 2006; Gobena *et al.*, 2017; Mohemed *et al.*, 2018). Two sorghum varieties, Shanqui Red (SQR) and SRN39, have been studied extensively in terms of the relationship between strigolactones and Striga resistance. SRN39 is a Striga-resistant improved sorghum variety released in Sudan, while SQR is a Chinese sorghum variety with high susceptibility to Striga (Satish *et al.*, 2012). SQR root exudate contains 5-deoxystrigol as the dominant strigolactone and has a high efficiency of Striga germination induction (Gobena *et al.*, 2017). SRN39 roots exude mainly orobanchol, leading to low Striga germination. This change in strigolactone exudation profile was associated with a deletion in the *LOW GERMINATION STIMULANT 1* (*LGS1*) locus (Satish *et al.*, 2012; Gobena *et al.*, 2017). *LGS1* encodes a putative sulfotransferase, but its role in strigolactone biosynthesis is not yet understood.

Several other sorghum genotypes possess the *lgs1* mutation and consequently have low Striga germination-inducing activity (Mohemed *et al.*, 2018; Bellis *et al.*, 2020). However, the *LGS1* loss-of-function alleles are not prevalent in Striga-prone regions and are absent from non-infested areas, which suggests potential trade-offs of *lgs1* mutations (Bellis *et al.*, 2020). Decreased expression of photosynthesis-related genes in root and shoot tissue of *LGS1* loss-of-function genotypes is one of the potential costs of Striga resistance (Bellis *et al.*, 2020). Moreover, elevated expression of genes involved in strigolactone biosynthesis in SRN39 roots indicates additional alterations of strigolactone profiles within this genotype, which were not previously captured in root exudate profiles (Bellis *et al.*, 2020). To date, it is not known whether the strigolactone composition of the root and shoot tissue reflects that of the root exudate. Strigolactones do pleiotropically regulate root and shoot architecture (reviewed in Aquino *et al.*, 2021), although it remains unknown whether the influence of strigolactones on plant development and metabolism varies with respect to different strigolactone structural variants.

Given the pleiotropic effect of strigolactones and the influence of LGS1 on strigolactone profiles and photosynthetic efficiency, one might expect that the *lgs1* genotypes would show differences in growth and plant architecture. However, only a minor reduction in leaf area was observed in the *lgs1* mutant (Bellis *et al.*, 2020), and the consequences of *LGS1* loss-of-function on sorghum growth and development have never been characterized in detail. Here, we use transcriptome profiling to identify biological processes that differentiate SQR and the *lgs1* genotype, SRN39. We show that genes involved in metabolism have altered expression in SRN39 as compared with SQR and further explore the phenotypic variation between these two varieties. Our results suggest that the consequences of the genetic differences between SQR and SRN39 for growth rate depend on plant developmental stage. We associate the reduced SRN39 shoot growth relative to SQR with increased accumulation of gibberellin precursors. We further characterize the root system architecture of several *lgs1* genotypes and speculate that various strigolactone structural variants affect root system architecture. Our results suggest that the differences between SQR and SRN39 go beyond distinct susceptibility to Striga, and include differences in growth, development, and root system architecture.

Materials and methods

Plant material

Seeds of *Sorghum bicolor* var. Shanqui Red (SQR) were obtained from GRIN (https://www.ars-grin.gov). Birhan, Framida, Gobiye, and SRN39 seeds were kindly donated by the Ethiopian Institute of Agricultural

Research. For each experiment seeds were surface sterilized by agitating in a solution containing 30% (v/v) commercial bleach and 0.2% Tween-20 (v/v) for 30 min followed by five washes with sterile water and overnight incubation in 5% (w/v) Captan fungicide. Sterilized seeds were germinated on wet Whatman paper (grade 1) upon incubation at 28 °C for 24 h in the dark.

Growth conditions and tissue collection for transcriptome and metabolome profiling

Four-day-old seedlings of approximately the same radicle length were transferred to a soil plug, i.e. a 50 ml falcon tube filled with sterile soil (soil collected from the Clue Field in the Netherlands; 52° 03′ 37.91″ N and 5° 45′ 7.074″ E, which was further dried, sieved through 4 mm mesh and sterilized by gamma irradiation) mixed with 5% sterile water (w/v). Seedlings were watered with autoclaved water every second day. On day 10, seedlings together with the soil plug were transferred to 40 cm-long cones (Greenhouse Megastore, cat. no. CN-SS-DP) filled with 700 ml of 0.5–1.0 mm filter sand (filcom.nl/). Plants were organized in a randomized manner in a greenhouse compartment with a temperature of 28 °C during the day (11 hours) and 25 °C at night (13 h), with 70% relative humidity and light intensity of 450 µmol m^{-2} s^{-1}. At days 0, 7 and 14, plants were watered with 50 ml of modified half-strength Hoagland solution with 0.05 mM KH_2PO_4. On days 1, 4, 10, 13, and 17, plants were watered with 50 ml deionized sterile water. Two and three weeks after transfer to the cones (corresponding to 28- and 35-day-old plants) root material was harvested 2 hours after the light turned on. Each sorghum plant was gently taken from the cone and the whole root system was cleaned from the sand and soil by washing in water, dried with paper towels, and snap frozen in liquid nitrogen (taking approximately 3 min per plant).

RNA-seq library preparation

Root tissue was manually ground and RNA was extracted with RNeasy Plus Mini kit (Qiagen) with application of QIAshredder columns (Qiagen) and on-column DNase I (Qiagen) treatment. Total RNA obtained was precipitated with 3 M NaOAc pH 5.2 (Thermo Fisher Scientific) in 100% ethanol and washed with 70% (v/v) ethanol. RNA-seq libraries were synthesized with QuantSeq 3′ mRNA-Seq Library Prep Kit (Lexogen) according to the manufacturer's protocol. Libraries were sequenced at the UC Davis DNA Technologies Core with Illumina HiSeq 4000 in SR100 mode with four biological replicates and three technical replicates for each RNA sample.

RNA-seq data processing and differential expression analysis

Quality control of resulting transcriptome sequencing data was accessed with FastQC (http://www.bioinformatics.babraham.ac.uk/projects/fastqc/) before and after read processing. Technical replicates of the libraries were pooled before reads were processed. Barcodes were trimmed from raw reads with fastx-trimmer (http://hannonlab.cshl.edu/fastx_toolkit/index.html) with parameters: -v -f 12 -Q33. Adaptor trimming and quality filtering was performed with reaper from Kraken Suite (Davis *et al.*, 2013) with options: -geom no-bc -tabu $tabu -3pa $seqAdapt -noqc -dust-suffix 6/ACTG -dust-suffix-late 6/ACTG -nnn-check 1/1 -qqq-check 35/10 -clean-length 30 -polya 5. Trimmed reads were mapped to the reference genome of *Sorghum bicolor* BTx623 (McCormick *et al.*, 2018) using STAR (Dobin *et al.*, 2013) with options: --outFilterMultimapNmax 20 --alignSJoverhangMin 8 --alignIntronMin 20 --alignIntronMax 10000 --outFilterMismatchNmax 5 --outSAMtype BAM SortedByCoordinate --quantMode TranscriptomeSAM GeneCounts.

Genes whose raw read counts across all samples equaled zero were removed. Counts per million (CPM) were calculated with the cpm() function from the edgeR package (Robinson *et al.*, 2010) and only genes with a CPM >1 in a minimum of three samples were used for further analysis. CPM values are found in Supplementary Table S1. Differentially expressed genes (DEGs) were identified with the R/Bioconductor limma package (Ritchie *et al.*, 2015). CPM values were normalized with the voom() function with quantile normalization to account for different RNA inputs and library sizes. The linear model for each gene was specified as an interaction of the genotype and the time point: log(counts per million) of an individual gene ~Genotype×Time. Differentially expressed genes for each term of linear model were selected based on a false discovery rate of <0.05. Lists of differentially expressed genes for each term (genotype, time, genotype-by-time interaction) are found in Supplementary Tables S2–S4.

Clustering analysis and ontology enrichment

Genes differentially expressed between genotypes in a time-dependent and time-independent manner were clustered in groups of genes that have similar expression patterns. The 75% most variable genes were selected for clustering. The $\log_2$ CPM mean across biological replicates was calculated for each gene and expression of each gene was then scaled to the mean expression across all samples. Hierarchical clustering was performed with pheatmap v.1.0.12 R package with the Euclidean distance measure to quantify similarity. Genes assigned to each cluster are listed in Supplementary Table S5.

Gene Ontology (GO) enrichment analysis was performed with the GOseq v.1.34.1 R package with a hypergeometric test (Young *et al.*, 2010). The odds ratio for each ontology was calculated with the formula: (number of genes in GO category/number of all genes in input)/(number of genes in GO category/number of genes in all clusters). Enriched ontology terms were selected based on a *P*-value <0.05 and an odds ratio >1. Multiple testing correction is not recommended for GO enrichment due to the graph structure of GO terms (Mi *et al.*, 2012). GO categories enriched in each cluster are listed in Supplementary Table S6.

Metabolomic analysis from 28- and 35-day-old plants

Root tissue was manually ground, and 70 mg of pulverized tissue was used for the extraction with 0.7 ml 80% methanol (v/v) containing 6×10^{-3} mg ml^{-1} ribitol (Sigma-Aldrich, St Louis, MO, USA) as internal standard. The mixture was shaken using a tissue-lyser (Tissuelyzer II, Qiagen) for 5 min at 30 Hz and subsequently sonicated for 5 min. Samples were centrifuged at 7600 relative centrifugal force at 10 °C for 5 min, and the supernatant was collected and filtered through a 0.22 µm-pore filter. Metabolite analysis by LC-MS was carried out as described in Melkonian *et al.* (2021) with slight modifications. Five microliters of root extract was injected in a Nexera ultra-high performance liquid chromatography (UHPLC) system (Shimadzu, Den Bosch, The Netherlands) coupled to a high-resolution quadrupole time-of-flight mass spectrometer (Q-TOF; maXis 4G, Bruker Daltonics, Bruynvisweg 16/18). Compounds were separated on a C18 stationary phase column (1.7 µm particle size, 150×2.1 mm; Acquity UPLC CSH C18, Waters, EttenLeur, The Netherlands) preceded by a guard column (1.7 µm particle size, 5×2.1 mm; Acquity UPLC CSH C18, Waters), a flow rate of 0.3 ml min^{-1}, and column temperature of 30 °C. Gradients of eluent A (0.1% v/v acetic acid in water) and eluent B (0.1% v/v acetic acid in 100% acetonitrile) were as follows: 0–1 min (5% B); 1–15 min (linear increase to 100% B); 15–18 min (100% B). Compound ionization was carried out by electrospray ionization operating in the negative mode using N_2 as the ionization gas with the following settings: capillary voltage 3500 V; end plate offset 500 V; nebulizer gas pressure (N_2) 1 bar; dry gas (N_2) 8 l min^{-1}; dry temperature 200 °C. Settings for MS analysis were: funnel radio frequency (RF) 200 voltage point to point (Vpp); multipole RF

200 Vpp; collision cell RF 200 Vpp; transfer time 40 µs; prepulse storage 5 µs. Internal mass calibration was performed automatically during every measurement by loop injection of 20 µl of a 2 mM sodium acetate solution in 1:1 v/v ultrapure water–isopropanol. Data acquisition was done using the Bruker Daltonics software suite Compass 2.7. Peak finding, peak integration and retention time correction were performed using the xcms R package version 1.38.0 (Smith *et al.*, 2006) after conversion of the original RAW files to an open-source format, 'mzXML', with the MSconvert tool from ProteoWizard version 3.0.5163 (Adusumilli and Mallick, 2017). The peak picking was performed using the 'centwave' method with the following parameters: Signal/Noise threshold=10, peakwidth=c (2, 24), mzdiff=0.001, prefilter=c (3, 100). The 'obiwarp' method was used for retention time adjustment. Finally, feature correspondence was achieved with the 'density' method using the following optimized parameters: bw=5.0 and mzwid=0.017. For pathway analysis, mzXML were imported into the xcms online web environment (Forsberg *et al.*, 2018) and analysed using the same parameters as described above. The sample BioSource was set to *Arabidopsis thaliana* var. Columbia for pathway annotation. Intensity values and abundance from 28- and 35-day-old plants can be found in Supplementary Tables S7–S9.

Root system architecture quantification from 28- and 35-day-old plants

Sorghum plants were gently taken from the pots, and roots were cleaned from the sand and soil by washing in water. Crown roots were separated from the seminal roots and fresh weight was scored for them separately. Roots were then placed in a water tray and scanned at 800 dpi resolution with Epson Perfection V700 scanner. Next, roots were dried with a paper towel, placed in paper bags, dried for 48 h at 65 °C and weighed to determine their dry weight. Root scans were analysed with the DIRT (Digital Imaging of Root Traits) software v1.1 (Das *et al.*, 2015). We used DIRT's area trait that counts the number of pixels representing the root in the image (Bucksch *et al.*, 2014) as a measurement for total root network area (to simplify we refer to it as total root length). Total network length (to simplify we refer to it as total root length) was computed by modifying the original code. As such, we count the number of pixels belonging to the medial axis of the network area after removing spurious medial branches whose medial circle radius at the tip is 2 pixels or smaller (Bucksch, 2014). Mean root network diameter was then calculated as the ratio of network area over network length. Values for each trait were transformed with natural logarithm transformation. A two-way ANOVA was used to determine the significance of the differences between genotype and genotype-by-time interactions with the following model: lm(trait~genotype×time) followed by a pairwise comparison with the formula: emmeans(model, specs=genotype×time, adjust='sidak'), with the emmeans v.1.5.2-1 R package.

Root system architecture quantification from seedlings

Germinated seeds of approximately the same radicle length were transferred to 25 cm-long (big pouches for SQR and SRN39 comparisons) or 18 cm-long (medium pouches for SQR and all *lgs1* genotypes) germination pouches (PhytoAb Inc., cat. no. CYG-38LG/CYG-98LB) filled with 17 ml or 50 ml autoclaved water, for medium and big pouches, respectively. Pouches were placed in the greenhouse with a maintained temperature of 26 °C and daylight of approximately 15 h. Pouches were scanned daily from the second to the seventh day after germination, approximately 11 hours after the start of the light period. The root system architecture of SQR and SRN39 was quantified at each time point imaged, while for the other *lgs1* genotypes (Framida, Birhan, Gobiye), root system architecture was only quantified in 7-day-old seedlings. Main root angle, main root length, lateral root number, and the length of individual lateral roots were quantified by manual tracing with ImageJ. Lateral root density was calculated as the ratio of lateral root number to main root length; lateral root length as a sum of the lengths of individual lateral roots; average lateral root length as the ratio of lateral root length to the number of lateral roots; and total root size as a sum of main and lateral root lengths. Prior to statistical analysis, data were transformed (square root transformation for the number of lateral roots, natural logarithm transformation for all the other traits, while the main root angle values were not transformed). The differences between genotypes at each individual time point were assessed with ANOVA including individual plant as a random factor with a formula: lmer(trait~Genotime+(1|Rep), data=x, REML=TRUE), where 'Genotime' indicates the combination of genotype and a time point (lme4 v.1.1-21 R package) followed with custom contrast comparison for two genotypes per time point with the formula: emmeans(model, specs=~Genotime, adjust='sidak'), where 'Genotime' indicates the combination of genotype and a time point (emmeans v.1.5.2-1R package). Seven to ten seedlings were used per genotype as biological replicates.

Exudate collection and strigolactone quantification

Seeds were surface sterilized by agitating in a solution containing 4% (v/v) sodium hypochlorite and 0.2% Tween-20 (v/v) for 30 min followed by three alternated washes with 70% ethanol (v/v) and sterile water. The disinfected seeds were thoroughly rinsed five times with sterile water and germinated on wet Whatman paper (grade 1) upon incubation at 28 °C for 48 hours in the dark. Germinated seeds with approximately the same radicle size were transferred to a 50 ml tube filled with washed river sand and perforated at the bottom to allow draining. The falcon tubes were covered with aluminum foil to prevent the roots from being exposed to light. The plants were grown for 14 days with a temperature of 28 °C during the day (11 hours) and 25 °C at night (13 hours), with 70% relative humidity and light intensity of 450 µmol m^{-2} s^{-1}. Seedlings were watered with modified Hoagland solution with low phosphate content (0.05 mM KH_2PO_4, 10% of the standard Hoagland content) to induce strigolactone exudation. Root exudate was collected from six plants for each of the sorghum genotypes. Each tube was flushed with 5% ethanol (v/v) in water to collect 35 ml of the flow-through. Each exudate sample was purified using solid phase extraction (SPE) with C18 Discovery cartridges (bed wt 500 mg, volume 6 ml, Merck). Cartridges were activated using 5 ml acetone and washed with 5 ml distilled water. Twenty milliliters of sample was loaded on the cartridge, which was further washed with 5 ml distilled water. Finally, compounds were eluted using 3 ml acetone. The acetone was evaporated using a SpeedVac (Scanvac, Labgene) and residual water was removed using freeze drying (Heto Powerdry LL1500, Thermo Fisher Scientific). The sample was reconstituted in 150 µl 25% (v/v) acetonitrile and filtered using a micropore filter (0.22 µm, 0.75 ml, Thermo Fisher Scientific) prior to UHPLC–tandem mass spectrometry analysis as described in (Floková *et al.*, 2020). Values for each compound abundances were transformed with natural logarithm transformation. One-way ANOVA was used to determine the significance of the differences between genotypes with the following model: lm(trait~genotype) followed by a Tukey *post hoc* test (adjusted P-value <0.05) with agricolae v.1.3-1 and multcompView v.0.1-8 R packages.

Growth analysis

Germinated seeds with approximately the same radicle length were transferred to pots containing a custom potting mix (one part coarse sand, one part compost, one part peat and 2.24 kg m^{-1} dolomite lime) and placed in the greenhouse with a maintained temperature of 26 °C and day light of approximately 15 hours. For each individual plant, every second day, starting from day 4, the number of leaves was counted and plant height measured (from the soil to the bend of the oldest leaf). The time to reach vegetative growth stages as defined in Vanderlip and Reeves (1972) was

scored. At the boot stage of each individual plant, when the boot length was approximately 20 cm, the shoot tissue was harvested and separated into leaves and stalk, roots were excavated from the soil and washed, and the fresh weight of each tissue was quantified. The tissue was then dried at 60 °C for 7 days and its dry weight measured. Ten plants with each plant as a biological replicate were tested for each genotype.

Statistics for growth analyses

The time required to reach individual growth stages was statistically assessed with a Wilcoxon test. Differences in biomass between genotypes were assessed using a Welch *t*-test. The increase in height of each plant was calculated as the slope of a linear curve fitted with a sliding window of 30 cm. The differences between genotypes in height or in the increase in height was assessed with a Welch *t*-test. The differences between genotypes in height per individual emerged leaf were assessed with ANOVA including individual plant as a random factor with formula: lmer(height~Genoleaf+(1|Pot), data=x, REML=TRUE), where 'Genoleaf' indicates genotype and leaf number combination (lme4 v.1.1-21 R package) followed with a custom contrast comparison for two genotypes for individual leaf number with formula: emmeans(model, specs=~Genoleaf, adjust='sidak'), where 'Genoleaf' indicates genotype and leaf number combination (emmeans v.1.5.2-1 R package). Phenotyping data can be found in Supplementary Dataset S1.

Results

SRN39 has altered expression of genes involved in metabolism and stress responses relative to Shanqui Red

Shanqui Red (SQR) and SRN39 are sorghum varieties commonly used as Striga-susceptible and -resistant models, respectively. Their potential differences in whole plant strigolactone composition as well as extensive genetic divergence suggest that additional differences in SRN39 growth and development should be characterized and considered in the interpretation of experiments using SRN39 and SQR as controls.

To gain insight into biological processes that may differ between these genotypes, we profiled the transcriptomes of 28- and 35-day-old plants, the approximate age used for sorghum strigolactone profiling (Gobena *et al.*, 2017; Mohemed *et al.*, 2018). As anticipated, given the extensive genotypic differences between these varieties (Gobena *et al.*, 2017), multidimensional scaling revealed a clear separation of transcriptional landscapes between the two genotypes, as well as an effect of plant age (Fig. 1A). Plant age influences the transcriptome of SRN39 roots to a greater extent than for SQR (Fig. 1A). We confirmed higher expression of several sorghum strigolactone biosynthetic genes in SRN39 compared with SQR (Supplementary Fig. S1), as previously observed by Bellis *et al.* (2020). Given the clear role of sorghum genotype and developmental age (time) in transcriptome variation, we used an ANOVA to identify genes whose expression differs depending on these factors (genotype, time and a genotype-by-time interaction; Supplementary Tables S2–S4). First, we identified genes whose expression was affected by the sorghum genotype, by time and in a time by genotype interaction (FDR threshold 0.05; Supplementary Table S2–S4). To further characterize these DEGs and their functions, we performed hierarchical clustering of genes affected by genotype itself or by a genotype-by-time interaction, resulting in identification of six co-expressed gene groups.

Genes in clusters 4 and 5 had similar expression at both time points in each genotype, but different respective expression between genotypes. In cluster 4, genes were expressed at lower levels in SRN39 relative to SQR while genes in cluster 5 had a higher magnitude of expression in SRN39 relative to SQR. Gene ontology enrichment ($P<0.05$ and odds ratio >1) suggests that these genes are associated with metabolism. For instance, in cluster 4, where expression is higher in SQR than SRN39, genes are associated with 'carbohydrate metabolic process' and 'phospholipid transport'. In cluster 5, genes are associated with the ontologies 'metabolic process', 'fatty acid biosynthetic process', and 'ammonium transport' (Fig. 1C, D). In contrast, expression of genes in cluster 3 decreased over time in both genotypes. Processes enriched within cluster 3 included 'response to stress', 'glucose catabolic process', and 'copper ion transmembrane transport' (Fig. 1C, D).

Genes with a more complex genotype-by-time interaction effect were found in clusters 1, 2, and 6. Genes from cluster 1, associated with 'response to water' and 'L-phenylalanine biosynthesis process' were more highly expressed in SRN39 at the later time point only (Fig. 1C, D). Genes with lower expression in SRN39 in 28-day-old plants but higher expression in 35-day-old plants (cluster 2) were enriched in 'defense response' and 'response to auxin'. Upon further inspection of the genes associated with these clusters, we found several genes related to auxin synthesis and transport: *Sobic.007G191400*, *Sobic.002G259100*, and *Sobic.004G156300* with homology to rice *OsSAUR50* (*SMALL AUXIN UP RNA 50*), *OsSAUR72*, and *OsSAUR72-like*, respectively (Supplementary Table S5) which could be linked to changes in plant growth and development. Genes involved in abscisic acid signaling, *Sobic.003G354000* and *Sobic.002G172000*, both with homology to Arabidopsis *HAI3* (*HIGHLY ABA-INDUCED PP2C PROTEIN*, *At2g29380*, Supplementary Table S5) were found among those influenced by a complex genotype-by-time interaction (Fig. 1C, D). SRN39 is grown predominantly in Sudan, often in non-irrigated fields. Thus, future research should focus on assessment of SRN39 responses to ABA in relation to drought responses, with consideration of plant age in this regulation.

SRN39 has altered gibberellin and fatty acid biosynthesis relative to Shanqui Red

The perturbations in expression of metabolism-related genes that we observed in SRN39 roots prompted us to profile the root metabolomes of SQR and SRN39 grown in the same set-up as for the transcriptome analysis. Similar to the transcriptome landscapes (Fig. 1A), the metabolite profiles of 28- and 35-day-old root of SQR and SRQ39 were clearly

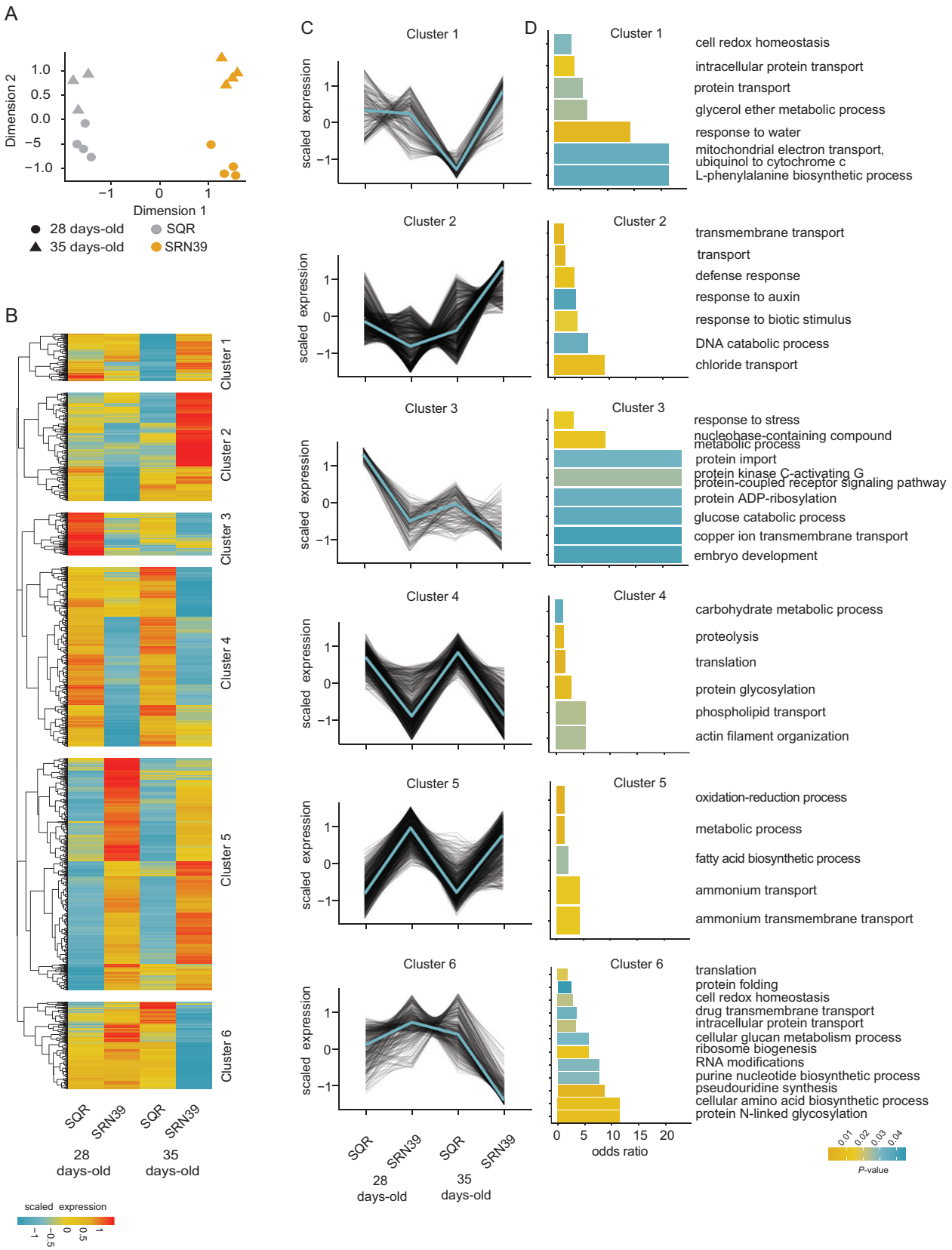

Fig. 1. Transcriptome profiles of roots of Shanqui Red (SQR) and SRN39. (A) Multidimensional scaling plot of samples based on their transcript abundances (log_2 counts per million, CPM). Gray, SQR; orange, SRN39; circles, 28 d old; triangles, 35 d old. (B, C) Six clusters of genes affected by a

separated and plant age had a more profound effect on metabolites of SRN39 than SQR (Fig. 2A). The metabolic features differentially accumulated between genotypes at both plant ages assessed were enriched with gibberellin biosynthesis (Fig. 2B, C). Several metabolic features predicted to be gibberellin precursors (ent-kaur-16-en-19-oate, ent-7α-hydroxykaur-16-en-19-oate, gibberellin A12-aldehyde, and gibberellin A12) had a higher abundance in roots of SRN39 than in SQR (Fig. 2D–H).

While we observed enrichment of genes associated with fatty acid biosynthesis to be more highly expressed in roots of SRN39 than SQR in both 28- and 35-day-old plants, metabolites involved in poly-hydroxy fatty acid biosynthesis and suberin monomer biosynthesis were perturbed only in 28-day-old roots. We observed higher levels of metabolic features predicted to be ferulate and *trans*-cinnamate in roots of SRN39 as compared with SQR (Fig. 2I, J). Ferulate and other phenylpropanoids are components of aliphatic suberin. In the roots of 35-day-old plants, a lower abundance of abscisic acid (Fig. 2K) complements observations of differential transcript accumulation of genes associated with ABA signaling. Collectively, our transcriptome and metabolome analysis demonstrate differences in hormonal balance between SQR and SRN39.

Differences in levels of gibberellin precursors and identification of complex gene expression interactions between 28- and 35-day-old SQR and SRN39 plants led to the hypothesis that complex differences in their plant growth may also be observed. Observation of the plants we sampled for transcriptome analysis suggest that such differences may occur. While most of the 28-day-old SQR and SR39 had five leaves, almost half of the 35-day-old SRN39 plant progressed to the six-leaf stage, and two-thirds of SQR plants remained in the five-leaf stage (Supplementary Fig. S2B). The SRN39 plants were shorter than SQR at both plant ages assessed (Supplementary Fig. S2A).

SRN39 root system architecture is distinct from Shanqui Red

Given the extensive genotype-by-time interactions in root gene expression between these genotypes, we asked whether this results in different root system architectures between these genotypes. We compared the total root system length and area, mean root network diameter and dry weight of 28- and 35-day-old plants grown in the same experimental set-up as used for transcriptome and metabolite profiling. Since strigolactones also play a role in the growth of shoot-borne roots (Kohlen *et al.*, 2012; Rasmussen *et al.*, 2012), we also quantified the above-mentioned traits separately for crown roots (shoot-borne roots) and seminal roots (roots of embryonic origin). The mean root network diameter of 28-day-old SRN39 plants was smaller than that of SQR plants of the same age, whereas in the case of 35-day-old plants, SQR displayed a higher mean root network diameter (Supplementary Fig. S2F). No significant differences were observed in the length and area of seminal roots, crown roots, and total root system (Supplementary Fig. S2C–N). These subtle time-dependent differences in root system architecture resemble the differences in gene expression observed between SRN39 and SQR occurring between the 28th and 35th day of growth (Supplementary Fig. S2B; Fig. 1A–C). The dry weight of seminal roots, but not crown roots or total root system size, was lower in the case of SRN39 than in SQR, independent of plant age (Supplementary Fig. S2C, G, K)

We further characterized changes in root system development in SRN39 and SQR seedlings from the second to seventh day after germination without nutrient supplementation. The SQR main root length was shorter than SRN39 from the very first days after germination and this difference increased over time (Fig. 3A). The main root of SQR deviated more from the gravity vector than the main root of SRN39 (Fig. 3B). While lateral root density was lower in SRN39 than in SQR from the fifth day after germination onwards (Fig. 3C), lateral root length was greater in SRN39 from the third day after germination (Fig. 3D). Although the increase in lateral root length was stable across multiple experiments, the magnitude of the difference in main root length was more variable (Figs 3A, D, 4A, B). Our observations suggest, therefore, that SRN39 has a longer and steeper main root, and longer lateral roots, compared with SQR at the seedling stage. Together this contributes to a greater total root system size of SRN39 as compared with SQR (Fig. 3E).

Sorghum genotypes producing orobanchol have increased lateral root growth

To verify whether the observed increase in root system size of SRN39 could be associated with the *LGS1* polymorphisms, or other genetic differences between SQR and SRN39, we evaluated the root system architecture of three other sorghum varieties: Birhan, Framida, and Gobiye. These genotypes carry a deletion of the same genomic region as SRN39, which spans five genes, including *LGS1* (Gobena *et al.*, 2017). SRN39, Birhan, Framida, and Gobiye all have the rare *lgs1-1* allele (Bellis *et al.*, 2020). The increased main root length was only found in Gobiye (Fig. 4A). All *lgs1-1* mutant varieties had an increase in average lateral root length (Supplementary Fig. S4B), total lateral root length (Fig. 4B) and total root system length (Fig. 4C) relative to SQR. We also confirmed

genotype in a time-dependent and -independent manner (B) and corresponding expression patterns (C). Values presented are $\log_2$CPM scaled to the mean expression across all samples. (D) Biological processes enriched in each cluster. The color of the bar indicates the *P*-value of the enrichment (at $P<0.05$ threshold). Root transcriptomes of four biological replicates were sequenced per genotype at each time point.

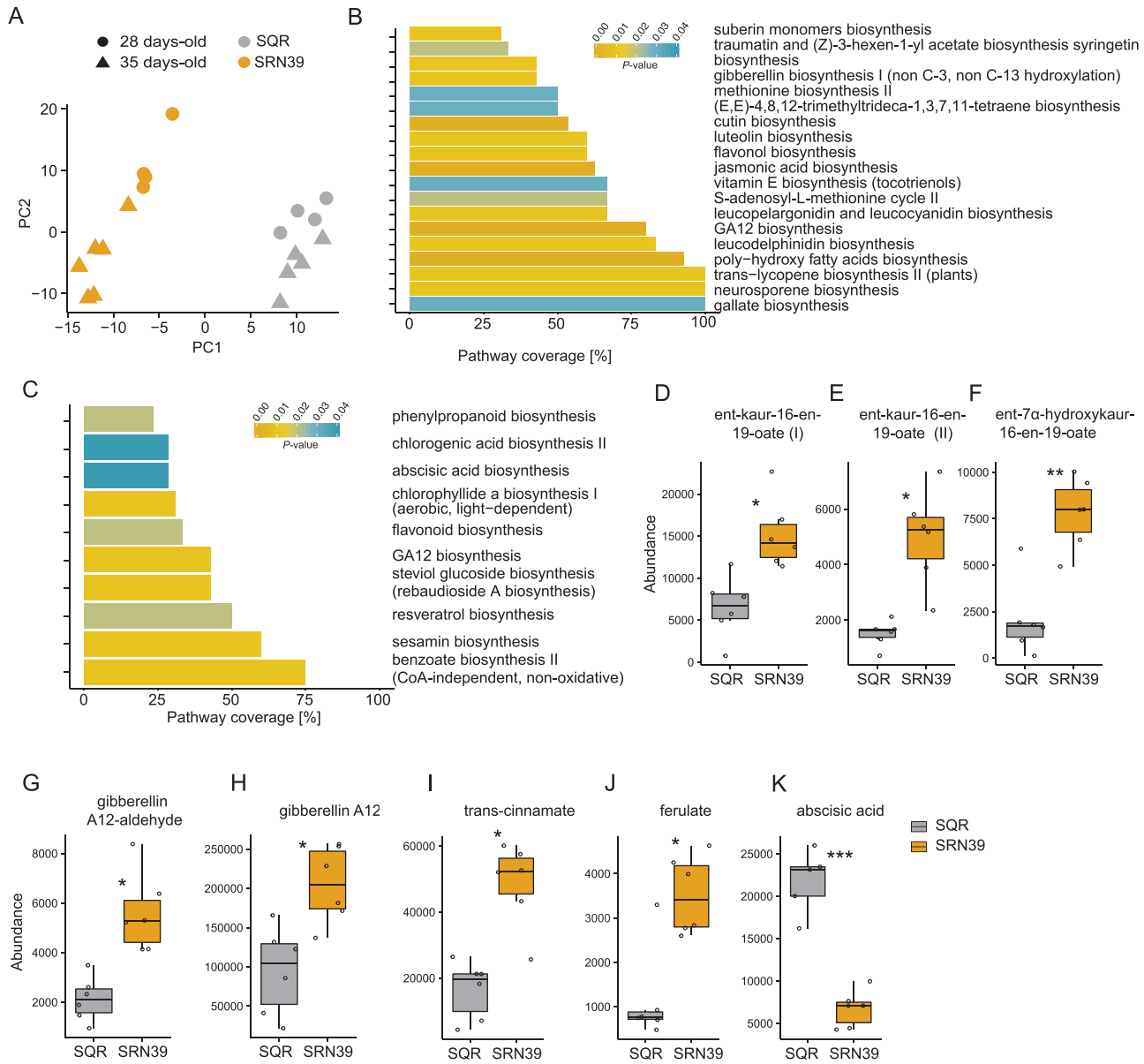

Fig. 2. Metabolome profiles of roots of Shanqui Red (SQR) and SRN39. (A) Principal component analysis of samples based on their metabolite abundance. Gray, SQR; orange, SRN39; circles, 28 d old; triangles, 35 d old. (B, C) Pathway enrichment analysis of metabolites differentially accumulated between genotypes at 28-day-old (B) and 35-day-old (C) stage. The color of the bar indicates the adjusted *P*-value of the enrichment (at the 0.05 threshold), while the *x*-axis indicates the proportion of the metabolites in each pathway that were found to be differentially accumulated in SRN39 as compared with SQR. (E–K) Abundance of gibberellin biosynthesis intermediates: metabolic features predicted to be ent-kaur-16-en-19-oate (D, E), ent-7α-hydroxykaur-16-en-19-oate (F), gibberellin A12-aldehyde (G), and gibberellin A12 (H); suberin intermediates: *trans*-cinnamate (I) and ferulate (J); and abscisic acid (K). Data in (D–J) present metabolite levels in roots of 28-day-old plants, those in (K) of 35-day-old plants. The boxplots denote data spanning from the 25th to the 75th percentile and are centered on the data median. Circles represent individual values. Asterisks denote a significant adjusted *P*-value for differences between genotypes by Student's *t*-test. **P*< 0.05, ***P*<0.01, ****P*<0.001 (*n*=6).

that, similar to SRN39, Birhan, Framida, and Gobiye varieties exuded orobanchol as a main strigolactone (Fig. 4D; Supplementary Fig. S5). We suggest that the deletion shared by these four genotypes may be associated with the promotion of lateral root growth, but whether it is the consequence of the *lgs1-1* mutation or other genetic components remains to be verified.

SRN39 is developmentally delayed, but accumulates more biomass

To evaluate whether the observed differences between SRN39 and SQR root transcriptomes and system architecture are concomitant with distinct growth and development of the above-ground tissue, we quantified SRN39 and SQR vegetative

growth in pots under standard greenhouse conditions over time. SRN39 plants were shorter than SQR, with the largest differences observed within the first 30 days of growth, after which the differences in plant height diminished, to increase again around day 70 (Fig. 5A). Most of the SRN39 plants did not reach the height of SQR at their respective boot stage (Fig. 5A). To determine whether the differences in height between SQR and SRN39 observed at the boot stage are caused by a decrease in growth specifically within early developmental stages we calculated the rate of height increase given individual plant height. SQR and SRN39 had a distinct growth rate for plants for heights up to 40 cm and for heights greater than 100 cm indicating that there are two phases of growth slow-down in SRN39 (Fig. 5B).

We next compared the time required for each genotype to reach specific stages of sorghum vegetative growth (Vanderlip and Reeves, 1972). Differences between SRN39 and SQR were observed at stage 1 (three-leaf stage), stage 4 (flag leaf visible) and stage 5 (boot stage). No differences were observed between SQR and SRN39 in the time required to reach stage 2 (five-leaf stage) and stage 3 (growing point differentiation) (Fig. 5C–G).

To verify whether the growth slow-down and developmental delay are coupled in SRN39, we compared the height of SRN39 and SQR relative to the emergence of each leaf. The differences in plant height between SRN39 and SQR were most prominent in the five-leaf stage (stage 2) and stage 3 (Fig. 5H). Given that there is no difference in the time to reach stage 2 and stage 3 between SQR and SRN39, a developmental delay cannot explain these final differences in plant height (Fig. 5D, E, H). Over the entire vegetative growth period monitored, most SRN39 plants developed a maximum of 13 leaves, while most SQR developed a maximum of 15 leaves (Fig. 5H). These collective data suggest that SRN39 is developmentally delayed at stage 1 only, while the later differences in growth between SRN39 and SQR are not due to a developmental delay.

We further assessed the biomass of the below- and above-ground (leaves and stalk) tissue in SRN39 and SQR. Consistent with the observed increase in RSA of SRN39 compared with SQR, the dry weight of the SRN39 root system was higher than that of SQR (Fig. 5I). No differences were observed in the dry weight of the shoot tissue (leaves and stalk together) (Fig. 1J), while the biomass of leaves was higher in SRN39 compared with SQR (Fig. 5K). The root biomass to shoot biomass ratio was also higher in SRN39 plants compared with SQR (Fig. 5L).

To summarize, while differences in early and late stages of vegetative growth (height) are observed between SRN39 and SQR, these are due to a developmental delay only at stage 1. A developmental delay is also observed at stages 4 and 5 in SRN39 relative to SQR (Fig. 5F, G). Despite being shorter and having fewer leaves (Fig. 5H), SRN39 allocates more biomass to its roots and leaves (Fig. 5I, K).

Discussion

Shanqui Red (SQR) is a Kaoliang-type sorghum variety of the bicolor race originating from China, while SRN39 is a released Sudanese variety of the caudatum race. SQR and SRN39 have been studied mostly in the context of their distinct levels of sensitivity to cold and Striga infection (Ejeta and Knoll, 2007). Despite their vast genetic diversity, the differences between these two genotypes have previously been attributed to a polymorphism in the *LGS1* locus leading to changes in composition of their root exudates (Gobena *et al.*, 2017). SQR exudes 5-deoxystrigol as its dominant strigolactone, while SRN39 produces only orobanchol (Gobena *et al.*, 2017) (Fig. 4D). 5-Deoxystrigol and orobanchol have distinct activity in terms of their stimulation of Striga germination. 5-Deoxystrigol is an efficient germination stimulant, while orobanchol only induces poor germination in most Striga seed populations (Gobena *et al.*, 2017). Consequently, SRN39 shows resistance to Striga in the field as opposed to the highly susceptible SQR (Mohamed *et al.*, 2003; Gobena *et al.*, 2017).

Since the determination of the *LGS1* contribution to Striga resistance, SQR and SRN39 have been routinely used as model genotypes in Striga research (Mohamed *et al.*, 2003; Gobena *et al.*, 2017). However, developmental and molecular consequences of the *LGS1* polymorphism as well as the extensive genetic divergence between SRN39 and SQR have never been addressed. Here we show that SRN39 has longer main and lateral roots, and greater overall root length than SQR in young seedlings (Figs 3, 5I). The enhanced growth of the main root and lateral roots in SRN39 seedlings was reflected in the higher total root biomass of mature plants, as compared with SQR (Figs 3A, D, 5I). The increased investment in root biomass accumulation might impair the growth of the above-ground plant organs (Lynch, 2007). We observed that both the growth and the development of SRN39 were affected when compared with SQR. SRN39 was delayed in reaching very early (stage 1, three-leaf stage), and late (stage 4, flag leaf visible; stage 5, boot stage) stages of vegetative growth and the growth rate (expressed as height) of its above-ground organs was also diminished at these stages (Fig. 5A–H). The increased investment in SRN39 root growth was observed at the early seedling stages and at the end of the vegetative growth, thus coinciding with the stages when the growth slow-down of the shoot was the largest and when developmental delay was observed: stage 1 (three-leaf stage), stage 4 (flag leaf visible), and stage 5 (boot stage) (Figs 3, 5B, C, F, G, I). The differences in root system architecture and root biomass were marginal in plants of five to six leaves (28- and 35-day-old plants), and thus at the stage where no developmental delay was observed for SRN39 plants and when its growth rate began to increase (Supplementary Fig. S2B–N; Fig. 5B, D). Together, these data suggest that the increased root growth of SRN39 is linked to both its developmental delay and reduced rate of above-ground growth. These differences between SRN39 and SQR could further be attributed to distinct molecular profiles.

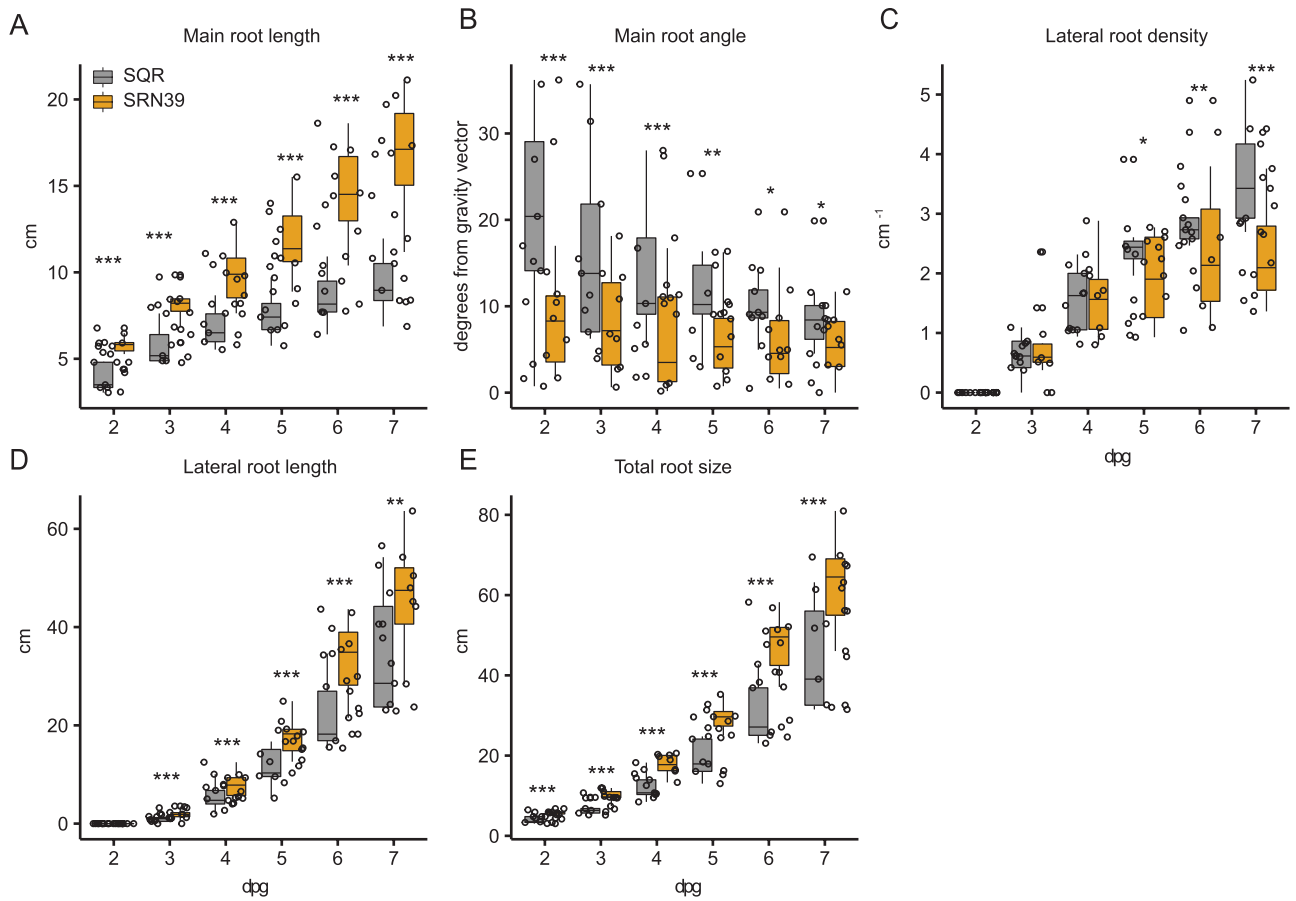

Fig. 3. Root system architecture of Shanqui Red (SQR) and SRN39. In all cases the *x*-axis denotes days post-germination (dpg). (A–E) SRN39, orange; SQR, gray. (A) Main root length, (B) main root angle, (C) lateral root density, (D) lateral root length, (E) total root size. The boxplots denote data spanning the 25th to the 75th percentile and are centered on the data median. Circles represent individual values. Asterisks denote a significant *P*-value for each time point between genotypes by the least square method. **P*< 0.05, ***P*<0.01, ****P*<0.001 (*n*=10).

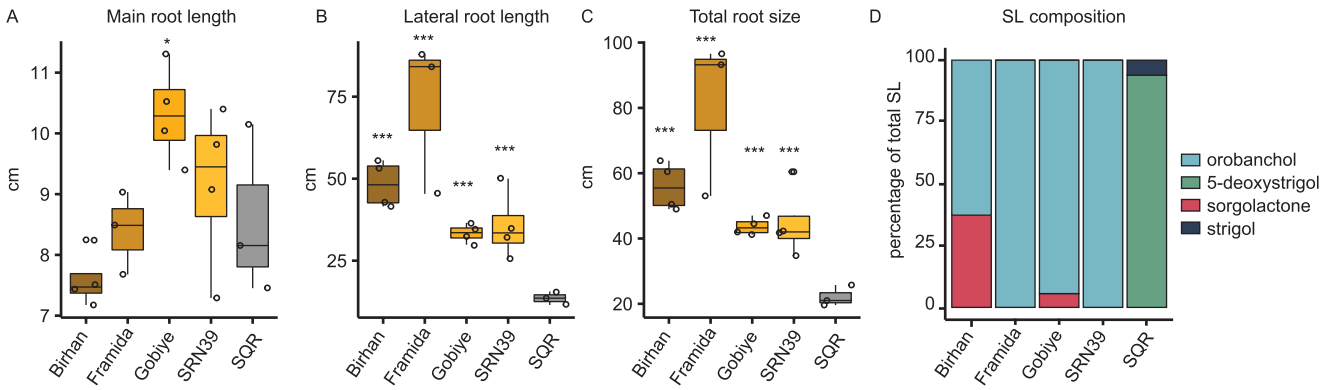

Fig. 4. Root system architecture and root exudate strigolactone composition of Shanqui Red (SQR) and sorghum varieties with the *lgs1* mutation (Birham, Framida, Gobiye, and SRN39). (A) Main root length, (B) lateral root length, (C) total root size of 7-day-old seedlings. The boxplots denote data spanning the 25th to the 75th percentile and are centered on the data median. Circles represent individual values. Asterisks denote a significant *P*-value for each time point between genotypes by the least square method. **P*< 0.05, ****P*<0.001 (*n*=4). (D) Relative abundance (percentage of total strigolactones (SL) measured) of four strigolactones in root exudates of 14-day-old plants (*n*=6). The abundance of individual strigolactones is presented in Supplementary Fig. S5.

The complex relationship between shoot and root growth over time in SRN39 was also reflected in the root transcriptomic and metabolic profiles. The effect of plant age on both the transcriptome and metabolome landscape was more profound in SRN39 than SQR (Figs 1A, 2A). Among the metabolic pathways perturbed in roots of SRN39 as compared with SQR,

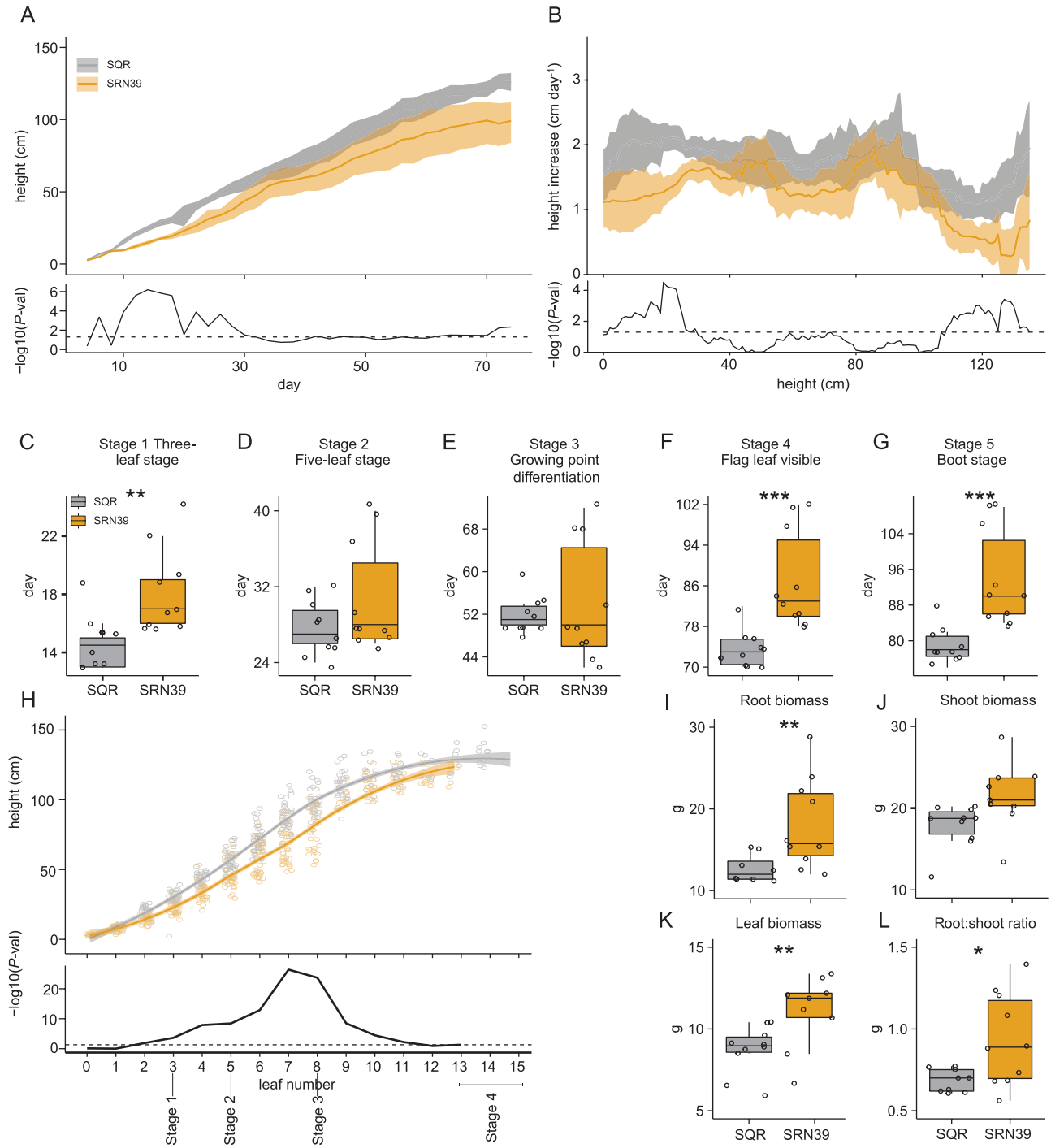

Fig. 5. Vegetative growth of SRN39 and Shanqui Red (SQR). (A) Plant height from day 4 to 74. (B) Increase in plant height per plant height calculated with a sliding window of 30 cm. Data presented include the mean (solid line) and the 95% confidence interval (shaded). The bottom panel denotes the $-\log_{10}$(*P*-value) at each time point (Welch's *t*-test). The dashed line indicates a *P*-value of 0.05. (C–G) Time required to reach stage 1 (three-leaf stage), (C) stage 2 (five-leaf stage) (D), stage 3 (growing point differentiation) (E), stage 4 (flag leaf visible) (F), stage 5 (boot stage) (G). An asterisk denotes the *P*-value from a Wilcoxon test. (H) Plant height at individual leaf stages. The mean is represented by a solid line, while the 95% confidence interval is shaded. The bottom panel denotes the $-\log_{10}$(*P*-value) per leaf stage as a result of pairwise genotype comparisons using the least square method. (I–L) Dry weight of root (I), stalk (J), leaves (K), and ratio of root to shoot dry weight (L). Boxplots denote the span from the 25th to the 75th percentile and are centered to the data median. Circles represent individual values. Asterisk denotes *P*-value from Welch *t*-test. **P*< 0.05, ***P*<0.01, ****P*<0.001 (*n*=10).

gibberellin biosynthesis was observed for 28- and 35-day-old plants (Fig. 2B, C). Several gibberellin precursors accumulated to higher levels in SRN39 as compared with SQR, which may be a reason why SRN39 plants are shorter than SQR (Fig. 2D–H). Recently Bellis *et al.* (2020) created a CRISPR-edited knock-out of *LGS1* in the Macia variety and profiled its shoot transcriptome. Two transcription factors involved in floral initiation, *Sobic.010G180200* and *Sobic.008G168400*, were differentially expressed in the shoot of a CRISPR-edited knock-out of *LGS1* as compared with the wild type, Macia (Bellis *et al.*, 2020), which could explain the delay in reaching a boot stage by SRN39 (Fig. 5G). Together, these results suggest that the growth slow-down and developmental delay of SRN39 plants may be attributed to decreased biosynthesis of active gibberellins and an increase of its precursors and altered expression of transcription factors controlling floral initiation, respectively.

Genes we identified as differentially expressed between SQR and SRN39 roots were enriched with processes related to metabolism ('carbohydrate metabolic process', 'metabolic process', 'fatty acid biosynthesis') and responses to biotic stimuli (Fig. 1C, D). Similar processes were enriched among genes differentially expressed in the CRISPR-edited *lgs1* knock-out and its wild type (Bellis *et al.*, 2020). Genes related to fatty acid biosynthesis had higher expression in roots of SRN39 than in SQR (Fig 1C, D, cluster 5). Consequently, among the metabolic pathways perturbed in SRN39 roots, we found poly-hydroxy fatty acid biosynthesis and suberin monomer biosynthesis (Fig. 2B, C). Suberin, a long chain fatty acid polymer, forms a protective barrier from pathogens (Thomas *et al.*, 2007; Andersen *et al.*, 2015; Holbein *et al.*, 2019) and may serve as an additional barrier from Striga parasitism in SRN39. Indeed, polymorphisms in genes associated with suberin and wax-ester biosynthesis were recently associated with levels of Striga occurrence (Bellis *et al.*, 2020), suggesting that, in addition to pre-attachment resistance, SRN39 may provide another layer of protection from Striga parasitism. Post-attachment resistance in SRN39 was previously suggested by Amusan *et al.* (2011). Genes involved in fatty acid biosynthesis were also enriched among genes differentially regulated in shoot tissue between the CRISPR-edited knock-out of *LGS1* and its wild type (Bellis *et al.*, 2020). While SRN39 plants were shorter than SQR, they also accumulated more leaf biomass, which could be due to the increased production of waxes (Fig. 5A, K).

The increased expression of genes related to fatty acid biosynthesis in both SRN39 and the CRISPR-edited *lgs1* knock-out leads to our hypothesis that strigolactones might affect suberin biosynthesis. More research is needed to confirm this hypothesis and to elucidate whether it is a direct effect of strigolactone signaling or an indirect effect of their exudation, i.e. on nutrient uptake. We cannot conclude which of the additional phenotypic and molecular differences demonstrated here are related to potential differences in strigolactone biosynthesis or exudation or to the extensive genetic variation between SQR and SRN39. The three other sorghum varieties, Birhan, Framida, and Gobiye, with the same *lgs1-1* allele as SRN39 and with orobanchol as the dominant exuded strigolactone, also showed longer lateral roots and larger root systems. Again, the mechanism underlying these differences remains to be determined. SRN39 is the parent of Birhan and Gobiye and therefore it is likely these two genotypes share a substantial part of the SRN39 genome (Hess and Ejeta, 1992). Nevertheless, our root system architecture phenotyping results suggest that these orobanchol-producing genotypes have a greater potential to promote lateral root growth than those producing 5-deoxystrigol. Previously, a synthetic strigolactone, GR24, has been shown to repress lateral root formation under phosphate-sufficient conditions, while enhancing it under conditions of low phosphate availability (Ruyter-Spira *et al.*, 2011). Here we suggest that, in the absence of nutrients, strigolactones might be also involved in the elongation of lateral roots. While more research is needed, we speculate that different stereoisomers of strigolactones may have distinct potential in shaping the sorghum root system.

SRN39 not only has increased resistance to Striga, but it is also Striga tolerant, meaning it has a reduced number of Striga infections and that successful Striga attachment causes minimal damage (Rodenburg *et al.*, 2005; Nasreldin, 2018). Striga tolerance is often measured as the degree of decrease in yield, photosynthesis efficiency, or above-ground tissue biomass (Van Ast *et al.*, 2000; Rodenburg *et al.*, 2008). We observed the dynamic character of the growth slow-down in SRN39, increases in leaf, but not whole shoot biomass and complex gene expression patterns over time that distinguish it from the *Striga*-sensitive SQR (Figs 1A–C, 5A, B, J, K). This suggests that accounting for the developmental stage and tissue used to access sorghum biomass might be important for assessing the tolerance of sorghum varieties with previously reported resistance to Striga.

Supplementary data

The following supplementary data are available at *JXB* online.

Fig. S1. Expression of strigolactone biosynthesis and signaling pathway genes in roots of 28- and 35-day-old plants of Shanqui Red (SQR) and SRN39.

Fig. S2. Phenotypic characterization of 28- and 35-day-old plants of Shanqui Red (SQR) and SRN39.

Fig. S3. Root system architecture of Shanqui Red (SQR) and SRN39.

Fig. S4. Root system architecture of 7-day-old seedlings of Shanqui Red (SQR) and sorghum varieties with the *lgs1* mutation (Birham, Framida, Gobiye, and SRN39).

Fig. S5. Strigolactone composition in root exudates of Shanqui Red (SQR) and sorghum varieties with the *lgs1* mutation (Birham, Framida, Gobiye, and SRN39).

Table S1. CPM values for root transcriptome profiling.

Table S2. Genes detected as differentially expressed between genotypes.

Table S3. Genes detected as differentially expressed between time points.

Table S4. Genes detected as differentially expressed between genotypes in a time-dependent manner.

Table S5. Genes assigned to expression clusters.

Table S6. GO terms enriched in each expression cluster.

Table S7. Intensity values for root metabolite profiling

Table S8. Abundance of metabolic features of selected enriched categories in roots of 28-day-old plants.

Table S9. Abundance of metabolic features of selected enriched categories in roots of 35-day-old plants.

Dataset S1. Raw data from the phenotyping experiments.

Acknowledgements

We would like to thank Peggy Lemeaux for her assistance in bulking Shanqui Red seeds, Ludek Tikovsky and Harold Lemereis for assistance in the greenhouse. We acknowledge Rick Helmus and Eva de Rijke (Institute for Biodiversity and Ecosystem Dynamics (IBED), University of Amsterdam) for their help with LC-QTOF analysis.

Author contributions

Conceptualization: DK, TT, BT, SMB. Data curation: DK, TT, BT. Formal analysis: DK, BT, AB. Funding acquisition: HB, SMB. Investigation: DK, TT, ZM, HEV, AW, SMB. Methodology: DK, BT, AB. Project administration: HB, SMB. Software: DK, BT, AB. Supervision: DK, BT, HB, SMB. Validation: DK, TT, BT, AW. Visualization: DK. Writing – original draft: DK, BT, AB, HB, SMB.

Conflict of interest

The authors have no affiliations with or involvement in any organization or entity with any financial interest in the subject matter or materials discussed in this manuscript.

Funding

This works was supported in whole by the Bill and Melinda Gates Foundation, Seattle, WA via grant OPP1082853 'RSM Systems Biology for Sorghum'. Under the grant conditions of the Foundation, a Creative Commons Attribution 4.0 Generic License has already been assigned to the author accepted manuscript version that might arise from this submission. SMB is partially funded by an HHMI Faculty Scholar grant. AB was in part supported by the USDOE ARPA-E ROOTS Award Number DE-AR0000821 and by the NSF CAREER Award No. 1845760 to AB. Any opinions, findings, and conclusions or recommendations expressed in this material are those of the author(s) and do not necessarily reflect those of the National Science Foundation.

Data availability

Sorghum sequences were deposited in NCBI GEO under the accession number GSE167101. Raw data from the growth measurements, root system architecture analysis, strigolactone measurements, ANOVA tables and *P*-values for each statistical test can be found in Supplementary Dataset S1. Data analysis scripts are publicly available at https://github.com/DorotaKawa/Sorghum-growth-development.git.

References

Adusumilli R, Mallick P. 2017. Data conversion with ProteoWizard msConvert. Methods in Molecular Biology **1550**, 339–368.

Akiyama K, Matsuzaki K, Hayashi H. 2005. Plant sesquiterpenes induce hyphal branching in arbuscular mycorrhizal fungi. Nature **435**, 824–827.

Amusan IO, Rich PJ, Housley T, Ejeta G. 2011. An in vitro method for identifying postattachment *Striga* resistance in maize and sorghum. Agronomy Journal **103**, 1472–1478.

Andersen TG, Barberon M, Geldner N. 2015. Suberization – the second life of an endodermal cell. Current Opinion in Plant Biology **28**, 9–15.

Aquino B, Bradley JM, Lumba S. 2021. On the outside looking in: roles of endogenous and exogenous strigolactones. The Plant Journal **105**, 322–334.

Awad AA, Sato D, Kusumoto D, Kamioka H, Takeuchi Y, Yoneyama K. 2006. Characterization of strigolactones, germination stimulants for the root parasitic plants *Striga* and *Orobanche*, produced by maize, millet and sorghum. Plant Growth Regulation **48**, 221–227.

Bellis ES, Kelly EA, Lorts CM, *et al.* 2020. Genomics of sorghum local adaptation to a parasitic plant. Proceedings of the National Academy of Sciences, USA **117**, 4243–4251.

Bouwmeester H, Li C, Thiombiano B, Rahimi M, Dong L. 2020. Adaptation of the parasitic plant lifecycle: germination is controlled by essential host signaling molecules. Plant Physiology **185**, 1292–1308.

Bouwmeester HJ, Roux C, Lopez-Raez JA, Bécard G. 2007. Rhizosphere communication of plants, parasitic plants and AM fungi. Trends in Plant Science **12**, 224–230.

Bucksch A. 2014. A practical introduction to skeletons for the plant sciences. Applications in Plant Sciences **2**, 1400005.

Bucksch A, Burridge J, York LM, Das A, Nord E, Weitz JS, Lynch JP. 2014. Image-based high-throughput field phenotyping of crop roots. Plant Physiology **166**, 470–486.

Das A, Schneider H, Burridge J, Ascanio AK, Wojciechowski T, Topp CN, Lynch JP, Weitz JS, Bucksch A. 2015. Digital imaging of root traits (DIRT): a high-throughput computing and collaboration platform for field-based root phenomics. Plant Methods **11**, 51.

Davis MP, van Dongen S, Abreu-Goodger C, Bartonicek N, Enright AJ. 2013. Kraken: a set of tools for quality control and analysis of high-throughput sequence data. Methods **63**, 41–49.

Dobin A, Davis CA, Schlesinger F, Drenkow J, Zaleski C, Jha S, Batut P, Chaisson M, Gingeras TR. 2013. STAR: ultrafast universal RNA-seq aligner. Bioinformatics **29**, 15–21.

Ejeta G, Gressel J. 2007. The *Striga* scourge in Africa: a growing pandemic. In: Ejeta G, Gressel J, eds. Integrating new technologies for *Striga* control. Singapore: World Scientific, 3–16.

Ejeta G, Knoll JE. 2007. Marker-assisted selection in sorghum. In: Varshney RK, Tuberosa R, eds. Genomics-assisted crop improvement: Vol 2: Genomics applications in crops. Dordrecht: Springer Netherlands, 187–205.

Floková K, Shimels M, Andreo Jimenez B, Bardaro N, Strnad M, Novák O, Bouwmeester HJ. 2020. An improved strategy to analyse strigolactones in complex sample matrices using UHPLC-MS/MS. Plant Methods **16**, 125.

Forsberg EM, Huan T, Rinehart D, Benton HP, Warth B, Hilmers B, Siuzdak G. 2018. Data processing, multi-omic pathway mapping, and metabolite activity analysis using XCMS Online. Nature Protocols **13**, 633–651.

Gobena D, Shimels M, Rich PJ, Ruyter-Spira C, Bouwmeester H, Kanuganti S, Mengiste T, Ejeta G. 2017. Mutation in sorghum *LOW GERMINATION STIMULANT 1* alters strigolactones and causes *Striga* resistance. Proceedings of the National Academy of Sciences, USA **114**, 4471–4476.

Hess DE, Ejeta G. 1992. Inheritance of resistance to *Striga* in sorghum genotype SRN39. Plant Breeding **109**, 233–241.

Holbein J, Franke RB, Marhavý P, Fujita S, Górecka M, Sobczak M, Geldner N, Schreiber L, Grundler FMW, Siddique S. 2019. Root endodermal barrier system contributes to defence against plant-parasitic cyst and root-knot nematodes. The Plant Journal **100**, 221–236.

Jamil M, Van Mourik TA, Charnikhova T, Bouwmeester HJ. 2013. Effect of diammonium phosphate application on strigolactone production and *Striga hermonthica* infection in three sorghum cultivars. Weed Research **53**, 121–130.

Kohlen W, Charnikhova T, Lammers M, *et al.* 2012. The tomato *CAROTENOID CLEAVAGE DIOXYGENASE8* (*SlCCD8*) regulates rhizosphere signaling, plant architecture and affects reproductive development through strigolactone biosynthesis. New Phytologist **196**, 535–547.

Lynch JP. 2007. Rhizoeconomics: The Roots of shoot growth limitations. HortScience **42**, 1107.

Mace ES, Tai S, Gilding EK, *et al.* 2013. Whole-genome sequencing reveals untapped genetic potential in Africa's indigenous cereal crop sorghum. Nature Communications **4**, 2320.

McCormick RF, Truong SK, Sreedasyam A, *et al.* 2018. The *Sorghum bicolor* reference genome: improved assembly, gene annotations, a transcriptome atlas, and signatures of genome organization. The Plant Journal **93**, 338–354.

Melkonian C, Fillinger L, Atashgahi S, *et al.* 2021. High biodiversity in a benzene-degrading nitrate-reducing culture is sustained by a few primary consumers. Communications Biology **4**, 530.

Mi G, Di Y, Emerson S, Cumbie JS, Chang JH. 2012. Length bias correction in gene ontology enrichment analysis using logistic regression. PLoS One **7**, e46128.

Mohamed A, Ellicott A, Housley TL, Ejeta G. 2003. Hypersensitive response to *Striga* infection in *Sorghum*. Crop Science **43**, 1320–1324.

Mohemed N, Charnikhova T, Fradin EF, Rienstra J, Babiker AGT, Bouwmeester HJ. 2018. Genetic variation in *Sorghum bicolor* strigolactones and their role in resistance against *Striga hermonthica*. Journal of Experimental Botany **69**, 2415–2430.

Nasreldin MA. 2018. The role of strigolactones in resistance, tolerance and control of Striga infection in Sorghum. PhD Thesis, Wageningen University.

Neumann E, George E. 2004. Colonisation with the arbuscular mycorrhizal fungus *Glomus mosseae* (Nicol. & Gerd.) enhanced phosphorus uptake from dry soil in *Sorghum bicolor* (L.). Plant and Soil **261**, 245–255.

Paterson AH, Bowers JE, Bruggmann R, *et al.* 2009. The *Sorghum bicolor* genome and the diversification of grasses. Nature **457**, 551–556.

Rasmussen A, Mason MG, De Cuyper C, *et al.* 2012. Strigolactones suppress adventitious rooting in Arabidopsis and pea. Plant Physiology **158**, 1976–1987.

Ritchie ME, Phipson B, Wu D, Hu Y, Law CW, Shi W, Smyth GK. 2015. Limma powers differential expression analyses for RNA-sequencing and microarray studies. Nucleic Acids Research **43**, e47.

Robinson MD, McCarthy DJ, Smyth GK. 2010. edgeR: a Bioconductor package for differential expression analysis of digital gene expression data. Bioinformatics **26**, 139–140.

Rodenburg J, Bastiaans L, Schapendonk AHCM, van der Putten PEL, van Ast A, Dingemanse NJ, Haussmann BIG. 2008. CO_2-assimilation and chlorophyll fluorescence as indirect selection criteria for host tolerance against *Striga*. Euphytica **160**, 75–87.

Rodenburg J, Bastiaans L, Weltzien E, Hess DE. 2005. How can field selection for *Striga* resistance and tolerance in sorghum be improved? Field Crops Research **93**, 34–50.

Ruyter-Spira C, Kohlen W, Charnikhova T, *et al.* 2011. Physiological effects of the synthetic strigolactone analog GR24 on root system architecture in Arabidopsis: another belowground role for strigolactones? Plant Physiology **155**, 721–734.

Satish K, Gutema Z, Grenier C, Rich PJ, Ejeta G. 2012. Molecular tagging and validation of microsatellite markers linked to the low germination stimulant gene (*lgs*) for *Striga* resistance in sorghum [*Sorghum bicolor* (L.) Moench]. Theoretical and Applied Genetics. **124**, 989–1003.

Smith CA, Want EJ, O'Maille G, Abagyan R, Siuzdak G. 2006. XCMS: processing mass spectrometry data for metabolite profiling using nonlinear peak alignment, matching, and identification. Analytical Chemistry **78**, 779–787.

Spallek T, Mutuku M, Shirasu K. 2013. The genus *Striga*: a witch profile. Molecular Plant Pathology **14**, 861–869.

Thomas R, Fang X, Ranathunge K, Anderson TR, Peterson CA, Bernards MA. 2007. Soybean root suberin: anatomical distribution, chemical composition, and relationship to partial resistance to *Phytophthora sojae*. Plant Physiology **144**, 299–311.

Van Ast A, Bastiaans L, Kropff MJ. 2000. A comparative study on *Striga hermonthica* interaction with a sensitive and a tolerant sorghum cultivar. Weed Research **40**, 479–493.

Vanderlip RL, Reeves HE. 1972. Growth stages of sorghum [*Sorghum-Bicolor*, (L) Moench]. Agronomy Journal **64**, 13–16.

Wang Y, Bouwmeester HJ. 2018. Structural diversity in the strigolactones. Journal of Experimental Botany **69**, 2219–2230.

Yoneyama K, Xie X, Kusumoto D, Sekimoto H, Sugimoto Y, Takeuchi Y, Yoneyama K. 2007. Nitrogen deficiency as well as phosphorus deficiency in sorghum promotes the production and exudation of 5-deoxystrigol, the host recognition signal for arbuscular mycorrhizal fungi and root parasites. Planta **227**, 125–132.

Young MD, Wakefield MJ, Smyth GK, Oshlack A. 2010. Gene ontology analysis for RNA-seq: accounting for selection bias. Genome Biology **11**, R14.